Mean-field theory of the morphology transition in stochastic diffusion-limited growth

Yuhai Tu
IBM T. J. Watson Research Center, P.O. Box 218, Yorktown Heights, New York 10598

Herbert Levine
Department of Physics and Institute for Nonlinear Science University of California, San Diego, La Jolla, California 92093-0402

(Received 9 May 1995)

We propose a mean-field model for describing the averaged properties of a class of stochastic diffusion-limited growth systems. We then show that this model exhibits a morphology transition from a dense-branching structure with a convex envelope to a dendritic one with an overall concave morphology. We also construct an order parameter that describes the transition quantitatively. The transition is shown to be continuous, which can be verified by noting the nonexistence of any hysteresis.

PACS number(s): 68.70.+w, 61.43.Hv, 47.20.Hw

I. INTRODUCTION

Diffusion-limited growth processes occur in a broad range of interesting systems ranging from physics to chemistry and to biology [1]. The common features that we observe in these systems are due to the patterns being driven by a generic instability that arises when the process of one phase replacing another phase is controlled by a diffusive field [2]. This instability leads to the breakdown of any simple shape and thereby causes the formation of complex interfacial structures. The structures that do form vary from smooth fingers to dendritic arbors to disordered, possibly fractal patterns in a manner dependent on the details of different individual systems.

Most of the work in this field has utilized one of two approaches. The first method relies on a continuum description of the interface evolution process, leading to a free surface problem for partial differential equations governing the diffusive transport. The models that one arrives at are purely deterministic; stochastic behavior can of course arise dynamically due to the inherent nonlinearities in the interfacial dynamics. A major success of this line of reasoning has been the discovery of the "microscopic-solvability" criterion, which enables us to understand the selection of a unique finger pattern out of an apparently continuous family of available solutions [1]. More recently [3], this approach has been used to study the global morphology of diffusion-limited solidification. From our perspective, studies of solidification using the phase-field method [4] fall into this same category; although quite different in computational detail from the sharp interface equations, these methods also embody deterministic microscopic models for interfacial evolution.

The second general scheme available to investigate diffusion-limited growth is the kinetic approach, where the diffusion field is represented by particles executing random walks. The boundary condition for the diffusive field and the local dynamics of the interface are combined into microscopic rules for these random walkers to stick to the aggregate cluster representing the growing "solid" phase. The simplest member of this class of models is diffusion-limited aggregation (DLA) [5], where the sticking rule is simply that the walker will become part of the aggregate upon contact with the aggregate. This simple model is known to produce a fractal structure and has been extensively investigated [6]. However, it is fair to say that a full theory of the relationship between the diffusive nature of the controlling field (walkers) and the fractal structure of the cluster that DLA generates still eludes us. Note that models of this second type are explicitly stochastic; whether this represents an important consideration or not is still an open question.

In order to study more realistic solidification processes, several groups have introduced more complicated local kinetics (sticking rules) and in addition have used a finite density of random walkers to mimic finite undercooling effects. Saito and Ueta [7] performed simulations of a many-walker model with Ising-like sticking probabilities. Liu and Goldenfeld [8] used a relaxation method in updating the walker distribution function (instead of using walkers per se), but chose a sticking rule that does not have any well defied thermodynamic limit. In a series of recent papers, Shochet *et al.* [9,10] have introduced the "diffusion-transition scheme," in which they have combined these above two ideas, i.e., directly solving for the walker distribution and using an Ising-like sticking probability at the interface. The main purpose of this study was to investigate the existence of different patterns as one changes the various control parameters, such as the density of the diffusive field at the boundary of the system (the undercooling), the chemical potential difference between the two phases (in a spin system analogy, this corresponds to a magnetic field favoring the solid phase), and the surface energy (bond energy, in the spin analogy).

In all the studies mentioned above, a morphology transition from a dense-branching morphology (DBM) to a dendritic structure has been observed. Locally, the DMB phase resembles the ramified structure of a DLA fractal, but at larger length scale, it is densely packed, i.e., it has a finite density and the pattern has a well-defined smooth envelop. For the dendritic phase, the directions of the

dendrites are determined by the anisotropy of either the surface energy or the interfacial kinetic coefficient. Due to the probabilistic nature of these models, each realization of the pattern looks different; in order to characterize the morphology transition, an ensemble average is used to study the statistical properties of the pattern distribution function. In terms of this ensemble-averaged pattern, the DBM to dendrite transition is connected to the change of the envelop shape from convex to concave.

Even though such a transition is quite well established in numerical simulations, there have been very few theoretical attempts to understand the transition [11]. Such a study is quite crucial if we are to answer questions regarding the role of explicit stochasticity, the possibility of morphology selection via a maximum velocity selection principle [12], and in fact the whole concept of a sharp transition between distinct morphologies.

Our goal here is to propose a mean-field theory (MFT) that describes the ensemble-averaged behavior of these stochastic models and more specifically the morphology transition. A mean-field theory is again a deterministic set of evolution equations, but these are meant to describe the average of the overall probability distribution and not any given realization; they should not be confused with the deterministic microscopic models mentioned above. In the next section, we describe our previous work on mean-field theories for the DLA sticking rule and how one can phenomenologically introduce mean-field reaction rates that lead to a better (i.e., more physically motivated) set of equations. Afterward, we explicitly discuss the issue of the nature of the morphology transition and conclude that in the mean-field treatment it is continuous. The final section contains a concluding discussion.

II. MEAN-FIELD EQUATIONS

In our previous work [13], we have studied the existence and nature of a morphology transition for the set of equations

$$\dot{\rho}=u(\rho^{\gamma}+a^2\nabla^2\rho) , \tag{1}$$

$$\dot{u}=D\nabla^2 u-\dot{\rho} , \tag{2}$$

where D is the diffusion constant, ρ is the density of the cluster, and u is the density of walkers, with the boundary conditions $u(\infty)=\Delta$, $\rho(\infty)=0$. Equation (2) arises due to the conservation of particles and the diffusive nature of the random walkers. Equation (1) is determined by the local kinetics of the growth process. Equations (1) and (2) were originally proposed to describe the ensemble-averaged behavior of the DLA without the $\dot{u}$ term in Eq. (2) and with different boundary condition for $u(\infty)$ [14]. The crucial difference between these equations and the original Witten-Sander DLA mean-field theory is that the phenomenological parameter γ is taken to be strictly greater than unity; later [15], this type of cutoff in the growth rate at small density was derived by proper inclusion of the average effects of the multiplicative noise that must be added to the naive reaction kinetics term so as to make a complete DLA theory. In that study [13], we did indeed discover that as one lowers the undercooling Δ, there is a morphology transition characterized by the change of the envelop shape from convex (DBM) to concave (dendrite). We did not find any discontinuity in the velocity slope versus Δ; this was subsequently verified to be true of the actual transition in many-walkers DLA [16].

It is obvious from Eqs. (1) and (2) that they cannot describe the kinetics of the more complex simulations; since the model was supposed to mimic the sticking rules of pure DLA, there is no parameter in the mean-field model playing the role of the chemical potential difference between the two phases. Finding an augmented set of equations is important because the aforementioned results on the continuous nature of the transition appear to disagree with the findings of the Shochet *et al.* diffusion-transition simulation. Also, a more physical model would obviate the need for the parameter γ since, as we shall see, a cutoff in growth at low density is an immediate consequence of the actual kinetics of these more realistic simulations.

We now turn to construction of the present mean-field model. One way of understanding the crucial feature that we need to include is by recognizing that the local kinetics satisfy detailed balance. The local-energy functional that governs this balance is determined by both the surface energy and the chemical potential difference between the two phases. Thus both the solidification of the liquid and the melting of the solid occur simultaneously with their rates dependent on this local-energy functional. This leads immediately to the form of the simplest MFT as

$$\dot{\rho}=(1-\rho)R_s(\Delta E,\mu_s,u)-\rho R_m(\Delta E,\mu_s,u) , \tag{3}$$

$$\dot{u}=D\nabla^2 u-\dot{\rho} . \tag{4}$$

The first term on the right-hand side of Eq. (3) represents the product of the probability of the site being empty $(1-\rho)$ and the rate of solidification $R_s(\Delta E,\mu_s,u)$; similarly, the second represents the product of the probability of the site being occupied by solid ρ and the rate of melting $R_m(\Delta E,\mu_s,u)$. Here ΔE is the local surface energy and μ_s is the chemical potential difference between the two phases.

In the actual kinetic simulation, the surface energy can depend on the detailed geometry of the solid near the vicinity of a possible site for melting or solidifying. In the mean-field description, ΔE at site i will be taken to depend on $\bar{\rho}_i$, which is the average of all nearest-neighbor densities at site i. In the continuum limit, $\bar{\rho}=\rho+(a^2/2d)\nabla^2\rho$, where a is the lattice spacing and d is the dimension. There is no analytic derivation for the explicit form of $\Delta E(\bar{\rho})$; however, we know that $\Delta E\to\infty$ as $\bar{\rho}\to 0$ in order to suppress the nucleation process inside the liquid phase and $\Delta E\to-\infty$ as $\bar{\rho}\to 1$ to suppress melting inside the solid. Also $\Delta E=-2B,0,2B$ when $\bar{\rho}=\frac{1}{4},\frac{1}{2},\frac{3}{4}$, which reflects the fact that when a site has 1, 2, or 3 neighbors being occupied, the bond energy gain energy for this site to be occupied is $2B$, 0, or $-2B$. We have chosen an expression for ΔE that satisfies the above requirements:

$$\Delta E(\bar{\rho}_i)=2B/\tan(\pi\bar{\rho}_i) . \quad (5)$$

We stress that the explicit form of $\Delta E(\bar{\rho}_i)$ is chosen for convenience once we ensure that it has sensible limits. It will become clear later in the paper that the detailed form of ΔE is unimportant for the qualitative behavior of the system, which in any even is all MFT can offer. Once we have an expression for ΔE, the simplest choices for the transition rates are

$$R_s(\Delta E,\mu_s,u)=\frac{u}{1+\exp(\Delta E-\mu_s)} ,$$
$$R_m(\Delta E,\mu_s,u)=\frac{1}{1+\exp(-\Delta E+\mu_s)} ; \quad (6)$$

$$R_s(\Delta E,\mu_s,u)=\frac{u}{u+\exp(\Delta E-\mu_s)} ,$$
$$R_m(\Delta E,\mu_s,u)=\frac{1}{1+u\exp(-\Delta E+\mu_s)} , \quad (7)$$

in accordance with the algorithms used by Refs. [9] and [7], respectively. We can easily see that the ratio of the two transition rates is the same for the two algorithms; this is what matters for the morphology transition, as we will show later. For the rest of the paper, we will use scheme (6).

III. RESULTS

We have studied the above equations numerically for both one and two dimensions. We first present our results in one dimension. There are three variables that are important for the morphology transition, i.e., B, μ_s, and Δ. We choose to fix $B=0.7$ and $\Delta=0.7$ and vary the chemical potential μ_s. We find that there is a critical value $\mu_s^*(B,\Delta)$ such that when $\mu_s>\mu_s^*$ the dynamics approaches a steady state. That is, starting from any initial condition, the system settles into a state in which the solid phase replaces the liquid phase with a constant velocity and the profiles of the ρ and u fields are time independent in the comoving range. When $\mu_s<\mu_s^*$, there is no steady-state solution. Instead, the ρ field will grow up to the maximum density $\rho=1$, the profile of the liquid density is now time dependent, and the width of the u field increases with time. These two phases of Eqs. (3) and (4) are shown in Figs. 1(a) and 1(b).

Before describing our results for the more interesting two-dimension (2D) case, let us try to understand the above results. We look for steady-state solution of Eqs. (3) and (4), where the interface (or the front) moves with a certain velocity v and the shape of the field profile does not change with time. We transform to the comoving frame by the change of variable $z=x-vt$; Eqs. (3) and (4) become

$$-v\partial\rho/\partial z=\frac{u(1-\rho)}{1+\exp(\Delta E-\mu_s)}-\frac{\rho}{1+\exp(-\Delta E+\mu_s)} , \quad (8)$$

$$-v\partial\rho/\partial z=D\partial^2 u/\partial z^2+v\partial v/\partial z . \quad (9)$$

Equation (9) above can be integrated to give

$$\rho=\Delta-u-\frac{D}{v}\partial u/\partial z , \quad (10)$$

where the boundary conditions $\rho\to 0$ and $u\to\Delta$ (as $z\to\infty$) have been used. Next we consider the profiles of the ρ and u fields away from the front, where there is no spatial dependence, so

$$\frac{u(1-\rho)-\rho\exp(\Delta E-\mu_s)}{1+\exp(\Delta E-\mu_s)}=0 , \quad (11)$$

$$\rho+u=\Delta . \quad (12)$$

The solution of Eq. (11) is $\rho=0$ (recall that $\Delta E\to\infty$ as $\rho\to 0$), $\rho=1$ ($\Delta E\to-\infty$), or $u=[\rho/(1-\rho)]\exp(\Delta E-\mu_s)$ $(0<\rho<1)$. The latter nontrivial relation is plotted in Fig. 2 together with the straight line $\rho+u=\Delta$ in the u-ρ plane. For μ_s large enough, there are three fixed points A, B, and C determined by Eqs. (11) and (12). Their relative position is illustrated in Fig. 2; it can be easily seen that fixed points A and C are stable, whereas fixed point B is unstable and separates the attraction basin of the two stable fixed points. The fixed point A represents the liquid state where $\rho=0$ and $u=\Delta$ and the

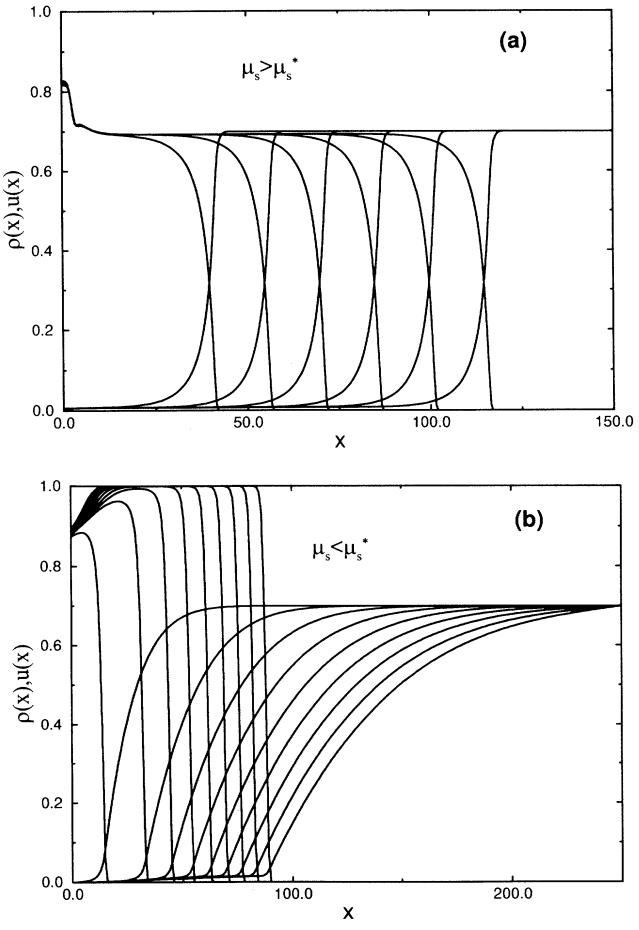

FIG. 1. 1D profiles of the aggregate and the walker fields with $\Delta=0.7$ and $B=0.7$ for (a) the "saturated phase" $\mu_s=6.8$ and (b) the "starved phase" $\mu_s=3.3$.

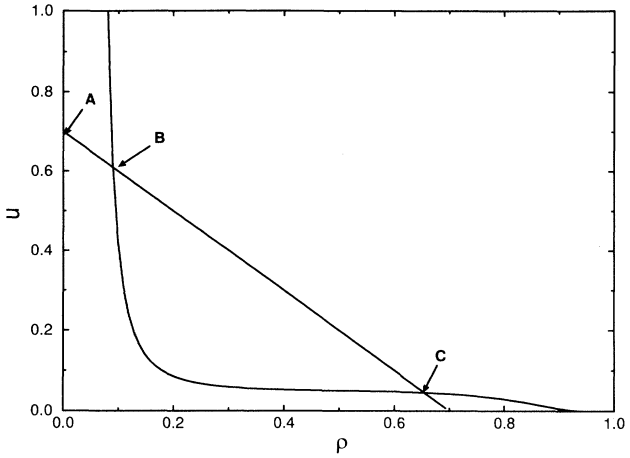

FIG. 2. Illustration of the fixed points of the dynamics. Fixed points A and C are stable and represent the liquid and the solid phases respectively, while fixed point B is unstable and separates the attraction basin of the two stable fixed points.

fixed point C with $\rho \sim \Delta$ and $u \ll \Delta$ describes the solid state.

It is well known in nonequilibrium systems [17] that when a stable state invades another stable state, the velocity of the front is uniquely determined. One way to see this is to substitute the solution of Eq. (10) into Eq. (8). We have an equation for just u:

$$D\partial^2 u/\partial z^2 + \left[v - \frac{D}{v} \frac{u + \exp(\Delta E - \mu_s)}{1 + \exp(\Delta E - \mu_s)} \right] \partial u/\partial z = \frac{u(1-\Delta+u) - (\Delta - u)\exp(\Delta E - \mu_s)}{1 + \exp(\Delta E - \mu_s)} . \quad (13)$$

The front velocity v is now a parameter in the above equation. By taking into account the asymptotic behavior of the u field at $z \to \pm\infty$, one can show that Eq. (13) is an eigenvalue equation for v, i.e., it is only solvable for a unique value of v.

At some critical plane in (μ_s, Δ, B) space, the fixed points B and C disappear together, which means that there is no steady-state growth possible in this regime. In fact, depending on the detailed functional form of ΔE, the steady-state solution disappears before the merging of B and C when there is no solution for the eigenvalue problem for any $v > 0$. This is the case for our choice of ΔE. In the regime where there is no steady state, the solid phase flows into the maximum density state with $\rho = 1$ [$\rho = 1$ is still a fixed point for Eq. (3)] and since the liquid phase only supplies a density of $u(\infty) = \Delta < 1$, there is a deficit in the u field. The u field tries to compensate for this deficit by getting particles from regions increasingly deeper into the liquid side with increasing time and thereby develops a time-dependent profile. We therefore call this phase of the dynamics the "starved phase" and the previous one the "saturated phase."

Having identified the two phases in one dimension, we can proceed to study the more important 2D case. We use the discretized version of Eqs. (3) and (4) using the grid size $\Delta x = \Delta y = a$, because any structure that is smaller than the lattice spacing a is unphysical. Let $a = 1$ and by writing $\bar{\rho}(i,j) = \frac{1}{4}[\rho(i+1,j) + \rho(i-1,j) + \rho(j+1,i) + \rho(j-1,i)]$ the surface energy anisotropy is automatically included in our model. The time step is chosen to be small $\Delta t = 0.01$. We find that both of the two phases found in one dimension have corresponding states in two dimensions. When the chemical potential is large, there is a 2D steady-state solution in which, in analogy with the saturated phase in one dimension, the solid phase has uniform density and the contour line separating the solid and liquid phase has a convex shape (deformed from a circle due to anisotropy). This phase can be identified as the DBM phase. The 2D starved phase becomes much more interesting due to the two dimensionality and the presence of anisotropy. Because of the surface energy anisotropy, the solid phase has four preferred growth directions (45° with respect to the lattice) in which to grow. As in the 1D case, the solid phase attempts to grow with maximum density $\rho = 1$ ($> \Delta$). However, due to the two dimensionality, the deficiency of supply can be compensated by the screening effect, by which the growth of solid in the preferred directions screens the growth in other direction and therefore a steady state can be reached. This possibility is directly connected to the existence of the Mullins-Serkerka instability. In fact, a stability analysis [18] for our previous model shows that there is indeed such instability for the flat interface in the dendritic phase. Qualitatively, for large μ_s, the liquid particle will become part of the solid upon contact with the solid aggregate and the cluster is essentially the same as finite density DLA, which belongs to the DBM morphology with not too small undercooling [13,16]. For small μ_s, the bond energy becomes important and the solid particles tend to stay together to take advantage of the bond energy and therefore form a density higher than Δ, which eventually causes the transition to dendrite morphology. A succession of snapshots of the morphology as we go through the transition by varying the chemical potential is shown in Fig. 3.

So far, we have shown that Eqs. (3) and (4) have a morphology transition in two dimensions between two phases whose origin can be related to the one-dimensional behavior of Eqs. (3) and (4). In order to better characterize the transition, we need to have an order parameter that describes the different macroscopic nature of the two different morphologies in analogy to what is normally done for an equilibrium phase transition. In [9], Shochet *et al.* proposed the front velocity as an order parameter; this was based on previous conjectures concerning the selection of coexisting patterns [12]. In their simulation, they showed that the dependence of the tip velocity on the chemical potential has a discontinuity of slope at the transition point (on a log-log plot). We have therefore measured the tip velocity versus the chemical potential for our model and the results are shown in Fig. 4(a). It is quite evident from the plot that there is no drastic change at the transition point, in agreement with the results of our previous model [13]. We as yet have no explanation for this discrepancy.

In general, a useful way to construct an order parameter in nonequilibrium systems is to first study the linear

stability of the system near the transition. Then the projection of the field onto the most unstable model or the amplitude of the most unstable mode can be used as an order parameter. This amplitude equation approach is useful in many nonequilibrium systems, including Rayleigh-Bénard convection and Taylor-Couette flow [17]. However, this weakly nonlinear methodology does not apply to our case, because dendritic growth is highly nonlinear. The initially most unstable mode strongly interacts with other unstable modes in the system and the scale of the final pattern is determined by the system size, not by the length scale set by the most linearly unstable mode. We are therefore forced to find some alternative way to construct an order parameter.

Given that the very nature of the transition is tied to the change of the spatial pattern, it seems natural to us to pick as a measure of the transition a quantity describing how the dendritic pattern picks up global correlation as compared to the DBM state. Recall that in the dendritic phase, the solid behind the front has a highly nonuniform density; we thus define our order parameter as the standard deviation of the solid density:

$$\psi=\sqrt{\langle\rho^2\rangle-\langle\rho\rangle^2} \tag{14}$$

with $\langle\rho^2\rangle=\int_\omega\rho^2 d\vec{x}/\int_\omega d\vec{x}$ and $\langle\rho\rangle=\int_\omega\rho\, d\vec{x}/\int_\omega d\vec{x}$.

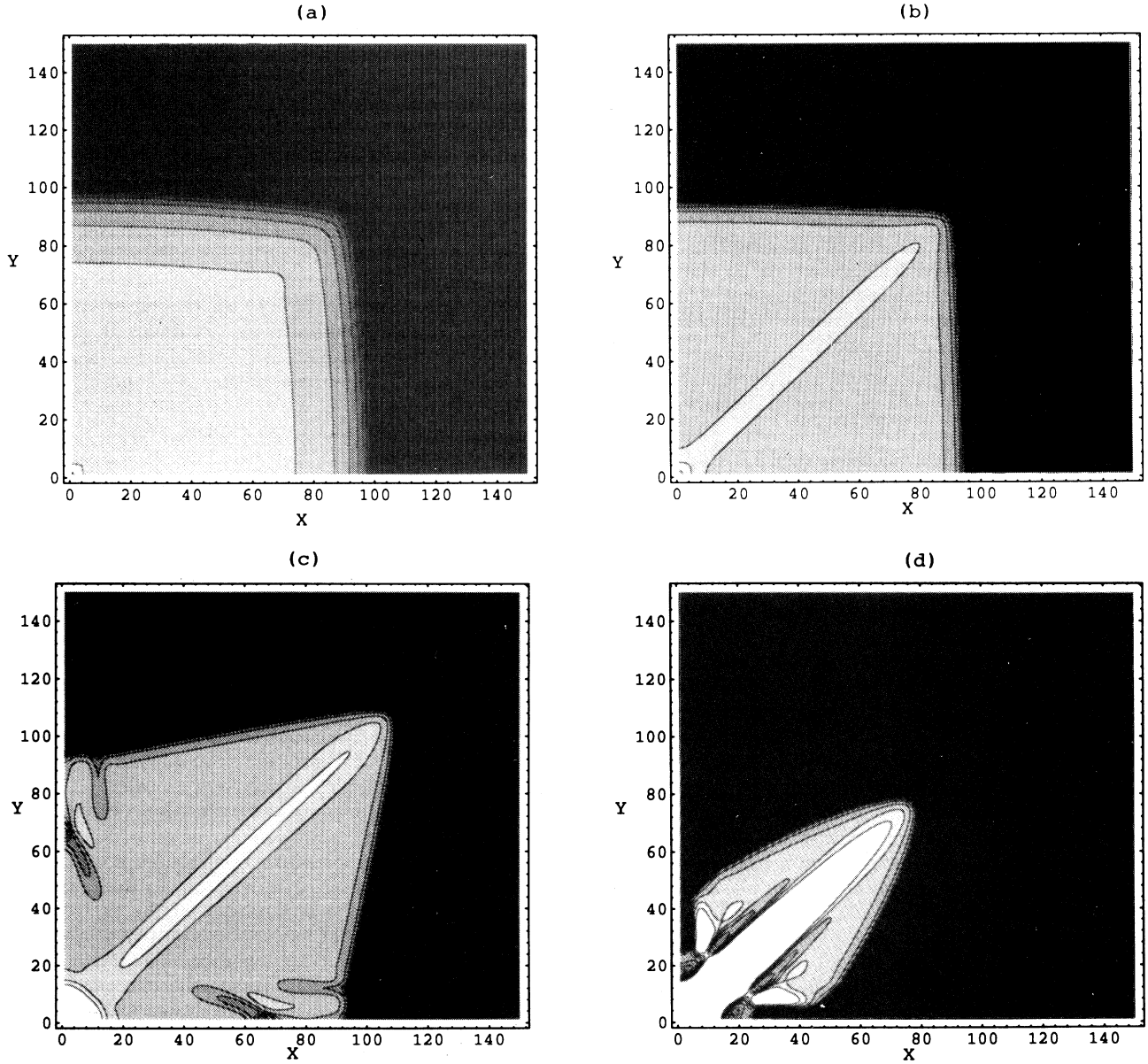

FIG. 3. Gray sale plot of the aggregate density field $\rho(X,Y)$. The darker region represents a smaller value of ρ. The contour lines are equally spaced in ρ between the maximum and minimum values of ρ. The morphology changes from a DBM (convex) to a dendrite (concave) with fixed $\Delta=0.7$ and $B=0.7$, as the chemical potential decreases: (a) $\mu_s=14.3$, (b) $\mu_s=5.8$, (c) $\mu_s=3.8$, and (d) $\mu_s=2.8$.

The integration region ω is the solid dominated region defined as where $u < \Delta/2$. This order parameter ψ is essentially the sum of the amplitude squares of all the modes. We have plotted the value of ψ versus the chemical potential in Fig. 4(b). It is quite evident from the figure that there is a continuous transition at around $\mu_s^* = 4.8$. From the above numerical results, we believe that the morphology transition (in our model) from the DBM phase to the dendritic phase is continuous.

To further clarify our results, we would like to comment on the simulations of Ref. [10], which claim to show the coexistence of the two distinct morphologies. In that reference, the authors performed simulations with the diffusion-transition scheme and confined the growth to a channel with the channel direction oriented 45° with respect to the preferred growth direction for possible dendrites. In the parameter range where one observes the dendrite phase in the open geometry, they obtained a different morphology that is similar to DBM. They

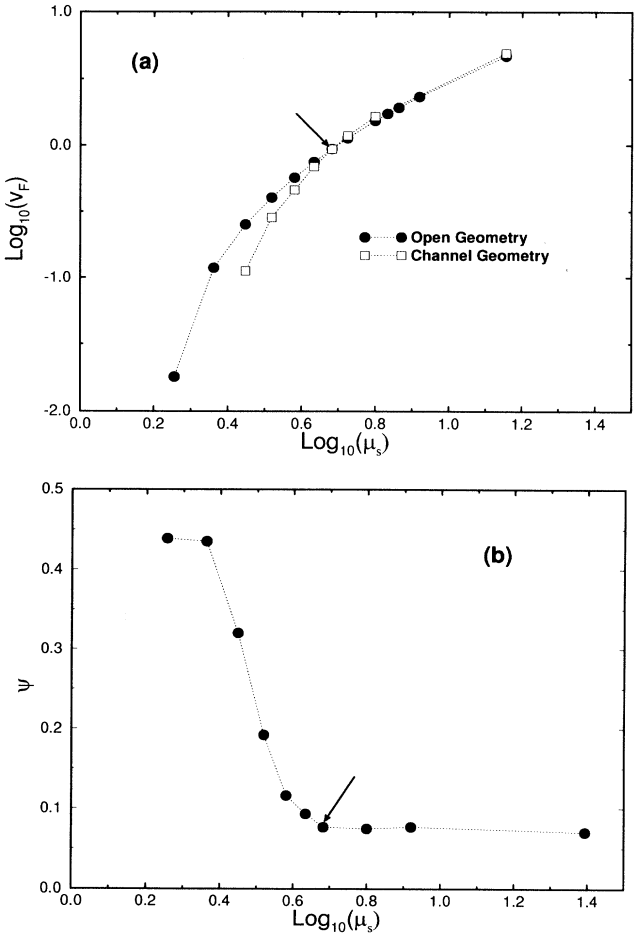

FIG. 4. (a) Front velocity v_F versus the chemical potential μ_s in a log-log plot. The filled circles are data for the open geometry; the open squares represent the front velocity measured in a channel geometry with channel width $W = 50$. The other parameters are fixed as in Fig. 3: $\Delta = 0.7$ and $B = 0.7$. The arrow indicates the morphology transition point. (b) The order parameter ψ as defined in the text versus the chemical potential.

therefore claimed that there exists some range of parameter where both the two phases are "available" and this coexistence is used to support the idea that the transition is discontinuous. However, because of the anisotropic nature of the dendritic phase, the boundary condition of the channel geometry in [10] has a very strong effect on the final pattern. It is therefore impossible to identify the existence of coexisting phases by using such an argument. One way to see this is to note that if one continuously changes the angle between the direction of the surface energy anisotropy and the boundary, one would see a continuous change of the front velocity; this certainly should not be attributed to the existence of a continuous family of morphologies.

To explicitly show how the channel results can be misleading, we have studied our mean-field model Eqs. (3) and (4) in the channel geometry with the lattice direction chosen to match the numerical experiment of Ref. [10]. We have used channel width $W = 50$ and channel lengths up to $L = 300$. In the parameter regime where the DBM exists, we see no change of front velocity as shown in Fig. 4(a). This is because the DBM phase is a local uncorrelated phase that is not affected by the boundary. When we decrease the chemical potential to the dendrite regime, the velocity of the front in the channel diverges from that in the open geometry, going below the previous curve. This is due to the strong interaction between the channel wall and the dendrites, which keep hitting the channel boundary and changing direction. In fact, this observation is very useful in identifying the actual morphology transition point; as we can see, the transition point determined by this method is the same as that determined by the order parameter ψ. On the other hand, it should not be interpreted as coexistence of the two phases, as our model has a continuous transition.

There is a standard and much more direct way to test whether a transition is continuous. We can adiabatically change the parameter across the transition point and determine whether there is any hysteresis. We prepare our system in the DBM regime very close to the transition point $\mu_s = \mu_s^*$, when we slowly change the chemical potential to lie below μ_s^*. The pattern immediately starts to generate dendrites at the edge of the previously disordered DBM pattern; these grow along the preferred direction and the forming of the dendrite takes over the entire dynamics. A series of plots showing this transition are given in Fig. 5. The chemical potential μ_s is decreased from $\mu_s = 5.8$ [Fig. 5(a)] to $\mu_s = 3.3$ [Fig. 5(d)]. The reverse process is observed with increasing chemical potential. We thus see no evidence for the existence of two attractors with different basins of attraction.

IV. SUMMARY

We have proposed a set of mean-field equations to describe the averaged behavior of a class of discrete diffusion-limited growth model. Although details of the microscopic kinetics will alter the detailed structure of our model, there are universal features that are independent of these details. We have shown that as long as

there are balancing effects between growth and melting, a 1D steady-state growing solution (the saturated state) will disappear at some critical point; instead, the 1D dynamics can be described by the spreading state, where the solid grows with the maximum density that is larger than the supply (the starved state). In two dimensions, these two phases become the DBM phase and the dendrite phase, respectively. The DBM phase is featureless and the density behind the front is uniform, whereas the dendritic phase organizes itself into a correlated structure, which then allows higher density in parts of the cluster than could be globally supplied by the liquid sate. From these properties of the two phases, we have constructed an order parameter, which is the measure of uniformity of the solid cluster. The behavior of the order parameter and nonexistence of hysteresis suggests that the transition is continuous.

Although we have discounted the purported numerical evidence for the coexistence of the DBM and dendritic phases, there still remains the discrepancy between our results on the velocity slope and those reported in the simulation studies. Assuming that both our results and these kinetic studies withstand further scrutiny, the only remaining possibility is that one cannot ignore fluctuation

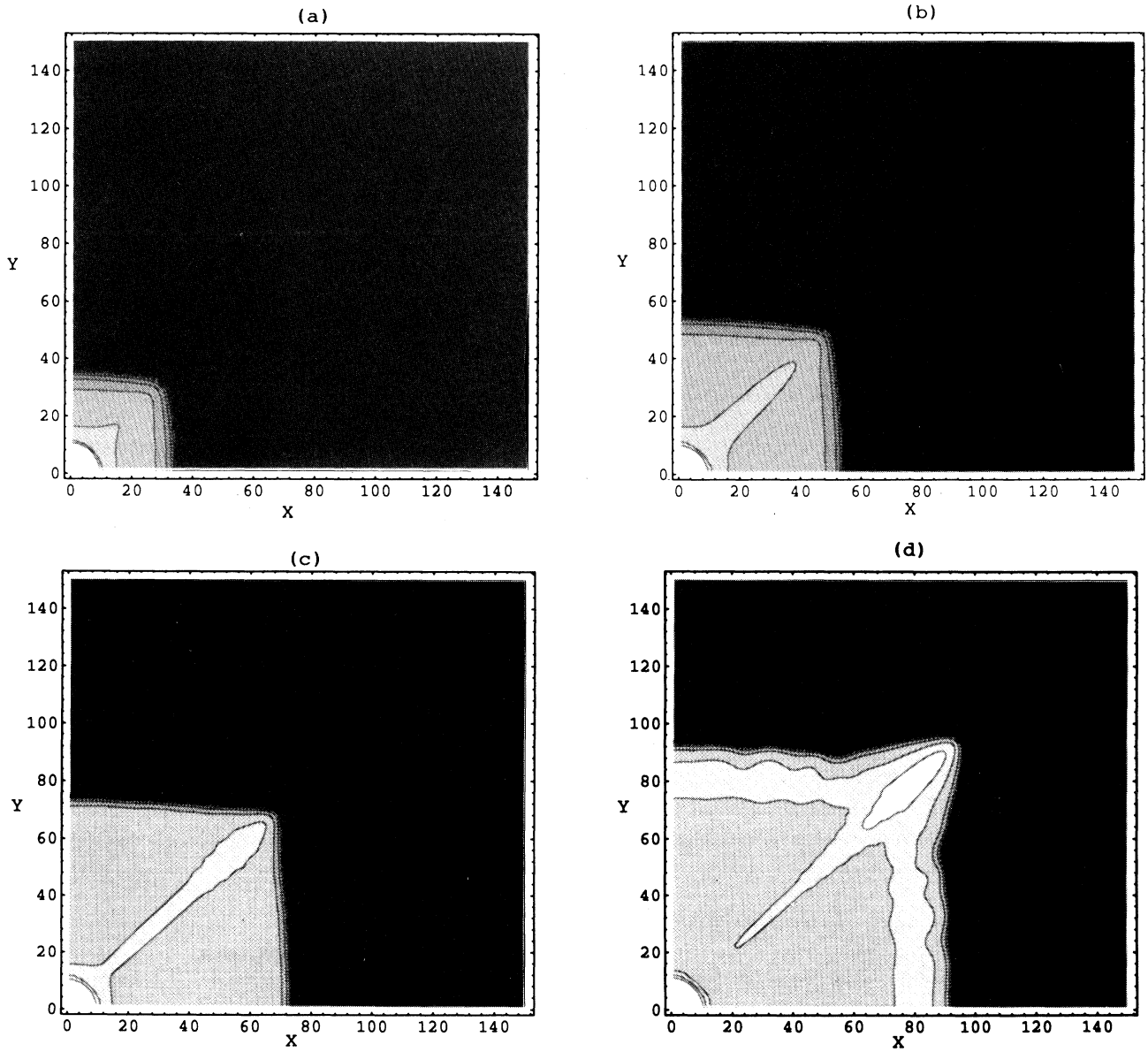

FIG. 5. Time series of gray scale plots of the 2D aggregate density field as the chemical potential is adiabatically changed from (a) above the critical value (the DBM regime) $\mu_s = 5.7$ to (b) below the critical value (dendrite regime) $\mu_s = 3.3$. (b) $\mu_s = 4.9$ and (c) $\mu_s = 4.1$. The contour lines are equally spaced in ρ between the maximum and the minimum values of ρ.

effects even insofar as determining the order of the transition. In any case, it is quite clear that mean-field approaches can only be used to obtain certain types of qualitative information: fluctuation effects are certainly important, probably independent of spatial dimensionality. Including these in a complete field-theoretic treatment of diffusion-limited growth remains a challenge for future work.

[1] There have been several reviews devoted to spatial pattern formation. See, e.g., D. Kessler, J. Koplik, and H. Levine, Adv. Phys. **37**, 255 (1988); P. Pelce, *Dynamics of Curved Fronts* (Academic, New York, 1988); J. Langer, in *Chance and Matter,* edited by J. Souletie (North-Holland, Amsterdam, 1987); E. Ben-Jacob and P. Garik, Nature **343**, 523 (1990); T. Vicsek, *Fractal Growth Phenomena* (World Scientific, Singapore, 1989).

[2] W. W. Mullins and R. K. Sekerka, J. Appl. Phys. **35**, 444 (1964).

[3] T. Ihle and H. Muller-Krumbhaar, Phys. Rev. E **49**, 2972 (1994); Phys. Rev. Lett. **70**, 3083 (1993).

[4] R. Kupferman, O. Shochet, E. Ben-Jacob, and Z. Schuss, Phys. Rev. B **46**, 16 045 (1992).

[5] T. Witten and L. M. Sander, Phys. Rev. Lett. **47**, 1400 (1981); Phys. Rev. B **27**, 5696 (1983); R. M. Ball, M. Nauenberg, and T. Witten, Phys. Rev. A **29**, 2017 (1984).

[6] For reviews of DLA see, e.g., P. Meakin, in *Phase Transitions and Critical Phenomena,* edited by C. Domb and J. L. Lebowitz (Academic, New York, 1988), Vol. 12, p. 336.

[7] Y. Saito and T. Ueta, Phys. Rev. A **40**, 3408 (1989).

[8] F. Liu and N. Goldenfeld, Phys. Rev. A **42**, 895 (1990).

[9] O. Shochet, K. Kassner, E. Ben-Jacob, S. G. Lipson, and H. Muller-Krumbhaar, Physica A **181**, 136 (1992); **187**, 87 (1992).

[10] O. Shochet and E. Ben-Jacob, Phys. Rev. E **48**, R4168 (1993).

[11] For one schematic attempt at understanding morphology phase diagrams, see E. Brener, H. Muller-Krumbhaar, and D. Temkin, Europhys. Lett. **17**, 535 (1992).

[12] E. Ben-Jacob and P. Garik, Nature **343**, 523 (1990); E. Ben-Jacob, P. Garik, T. Muller, and D. Grier, Phys. Rev. A **38**, 1370 (1988); E. Ben-Jacob and P. Garik, Physica D **38**, 16 (1989).

[13] Y. Tu, H. Levine, and D. Ridgway, Phys. Rev. Lett. **71**, 3838 (1993).

[14] E. Brener, H. Levine, and Y. Tu, Phys. Rev. Lett. **66**, 1978 (1991); H. Levine and Y. Tu, Phys. Rev. A **45**, 1044 (1992); **45**, 1053 (1992).

[15] H. Levine and Y. Tu, Phys. Rev. E **48**, R4207 (1993).

[16] O. Shochet, Phys. Rev. E **49**, 1005 (1994).

[17] M. Cross and P. Hohenberg, Rev. Mod. Phys. **65**, 851 (1993).

[18] D. Ridgway, H. Levine, and Y. Tu (unpublished).

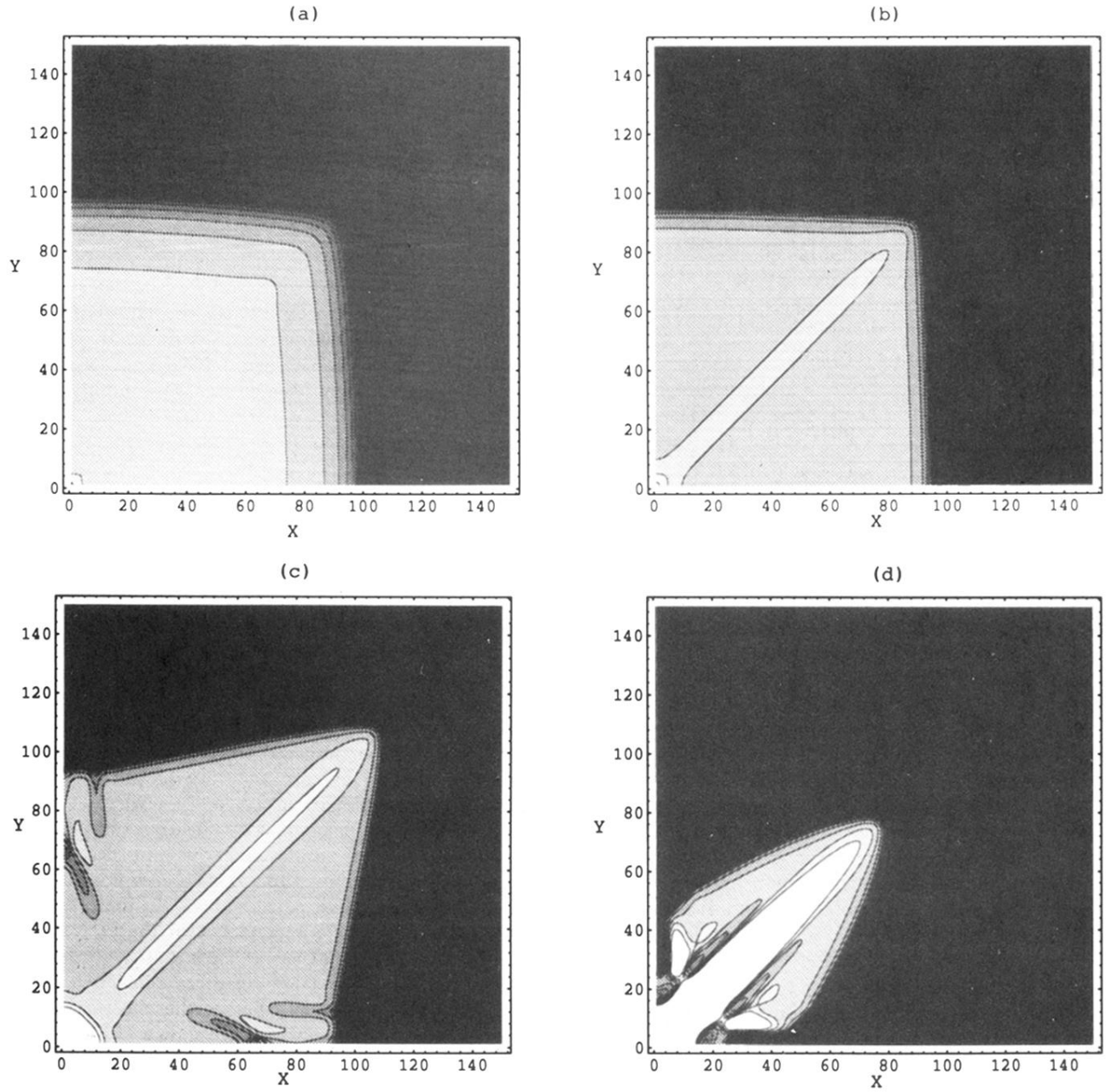

FIG. 3. Gray sale plot of the aggregate density field $\rho(X, Y)$. The darker region represents a smaller value of ρ. The contour lines are equally spaced in ρ between the maximum and minimum values of ρ. The morphology changes from a DBM (convex) to a dendrite (concave) with fixed $\Delta = 0.7$ and $B = 0.7$, as the chemical potential decreases: (a) $\mu_s = 14.3$, (b) $\mu_s = 5.8$, (c) $\mu_s = 3.8$, and (d) $\mu_s = 2.8$.

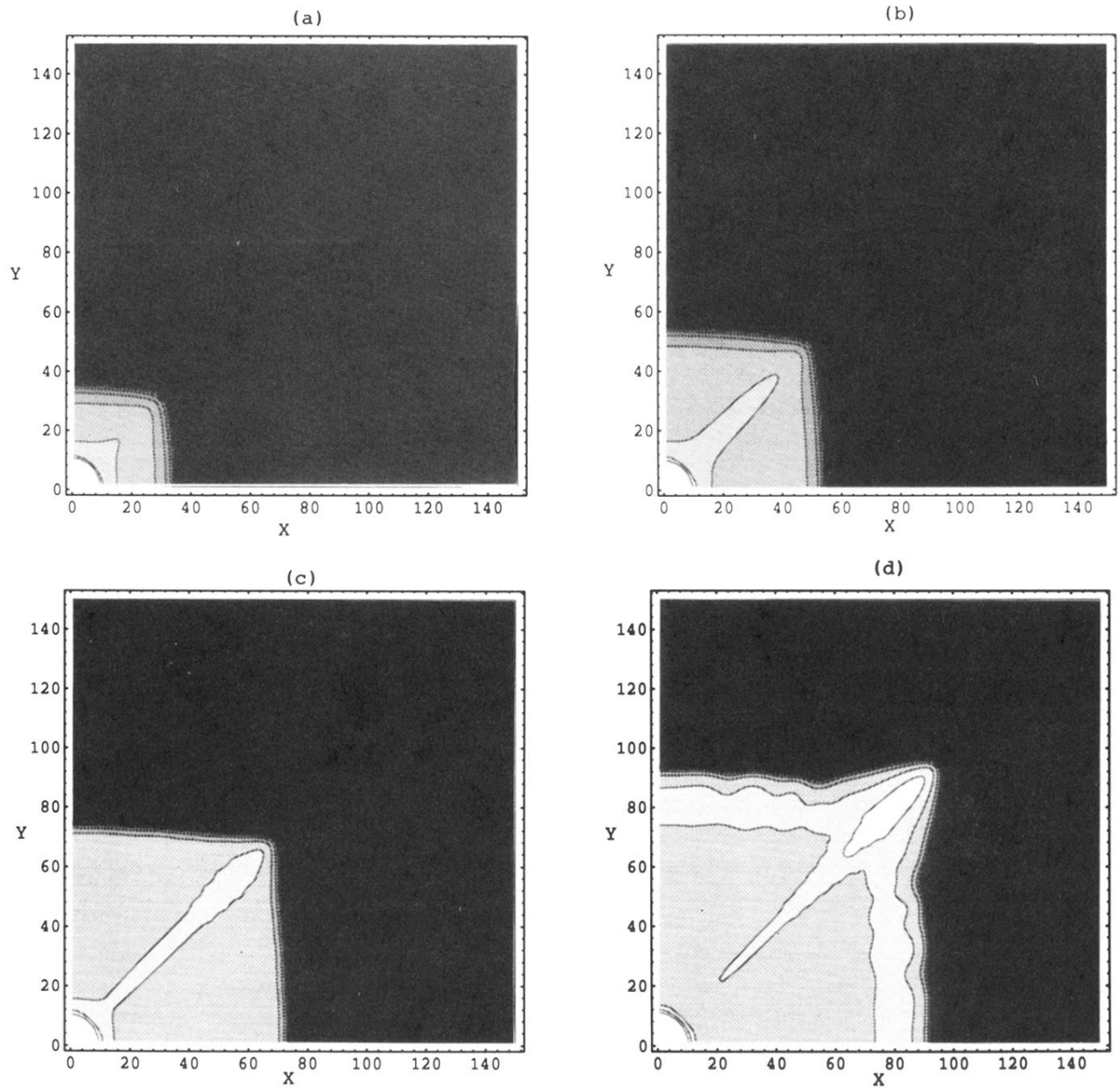

FIG. 5. Time series of gray scale plots of the 2D aggregate density field as the chemical potential is adiabatically changed from (a) above the critical value (the DBM regime) $\mu_s = 5.7$ to (b) below the critical value (dendrite regime) $\mu_s = 3.3$. (b) $\mu_s = 4.9$ and (c) $\mu_s = 4.1$. The contour lines are equally spaced in ρ between the maximum and the minimum values of ρ.